Retrieval of aerosol optical depth under thin cirrus from MODIS: Application to an ocean algorithm

Jaehwa Lee,[1,2] N. Christina Hsu,[2] Corey Bettenhausen,[2,3] and Andrew M. Sayer[2,4]

Received 22 July 2013; revised 27 August 2013; accepted 31 August 2013; published 12 September 2013.

[1] A strategy for retrieving aerosol optical depth (AOD) under conditions of thin cirrus coverage from the Moderate Resolution Imaging Spectroradiometer (MODIS) is presented. We adopt an empirical method that derives the cirrus contribution to measured reflectance in seven bands from the visible to shortwave infrared (0.47, 0.55, 0.65, 0.86, 1.24, 1.63, and 2.12 μm, commonly used for AOD retrievals) by using the correlations between the top-of-atmosphere (TOA) reflectance at 1.38 μm and these bands. The 1.38 μm band is used due to its strong absorption by water vapor and allows us to extract the contribution of cirrus clouds to TOA reflectance and create cirrus-corrected TOA reflectances in the seven bands of interest. These cirrus-corrected TOA reflectances are then used in the aerosol retrieval algorithm to determine cirrus-corrected AOD. The cirrus correction algorithm reduces the cirrus contamination in the AOD data as shown by a decrease in both magnitude and spatial variability of AOD over areas contaminated by thin cirrus. Comparisons of retrieved AOD against Aerosol Robotic Network observations at Nauru in the equatorial Pacific reveal that the cirrus correction procedure improves the data quality: the percentage of data within the expected error $\pm(0.03 + 0.05 \times \mathrm{AOD})$ increases from 40% to 80% for cirrus-corrected points only and from 80% to 86% for all points (i.e., both corrected and uncorrected retrievals). Statistical comparisons with Cloud-Aerosol Lidar with Orthogonal Polarization (CALIOP) retrievals are also carried out. A high correlation ($R = 0.89$) between the CALIOP cirrus optical depth and AOD correction magnitude suggests potential applicability of the cirrus correction procedure to other MODIS-like sensors.

Citation: Lee, J., N. C. Hsu, C. Bettenhausen, and A. M. Sayer (2013), Retrieval of aerosol optical depth under thin cirrus from MODIS: Application to an ocean algorithm, *J. Geophys. Res. Atmos.*, *118*, 10,111–10,124, doi:10.1002/jgrd.50806.

1. Introduction

[2] Atmospheric aerosols play a significant role in the Earth's climate system by regulating the radiation balance through direct, indirect, and semidirect effects [*Intergovernmental Panel on Climate Change*, 2007]. Due to their strong spatial and temporal variability, satellite observations have been recognized as a key research tool in understanding radiative forcing of aerosols with their high spatial and temporal coverage. Among the Earth-observing satellites, the Moderate Resolution Imaging Spectroradiometer (MODIS) instruments onboard the Terra and Aqua satellites have performed daily near-global measurements of top-of-atmosphere (TOA) radiance in 36 spectral bands ranging from 0.412 to 14.235 μm with spatial resolution of 250, 500, and 1000 m at nadir (depending on wavelength) and daytime local equatorial crossing time of 10:30 for Terra and 13:30 for Aqua. As one of the key retrieval parameters, MODIS has provided unprecedented information on aerosol optical properties, with algorithms making use of the measurements in the visible to shortwave infrared spectral range (0.412–2.12 μm), since the year 2000 for MODIS-Terra and 2002 for MODIS-Aqua [*Hsu et al.*, 2004, 2006; *Remer et al.*, 2005; *Levy et al.*, 2007]. The primary quantity retrieved by these algorithms is the midvisible aerosol optical depth (AOD).

[3] Aerosol remote sensing using shortwave bands from passive satellite radiometers such as MODIS and Sea-viewing Wide Field-of-view Sensor is typically limited to cloud-free areas, except in cases of absorbing aerosols above cloud layers [e.g., *Hsu et al.*, 2003; *Torres et al.*, 2012; *Jethva et al.*, 2013]. Under cloudy conditions, AOD retrievals can be contaminated by the strong reflectance of clouds, and the magnitude of this contamination depends on the intensity of the cloud contribution to TOA reflectance [*Kaufman et al.*, 2005]. Although cloud detection procedures in AOD retrieval algorithms are effective at reducing contaminations caused from optically thick clouds, they can fail to detect optically thin cirrus clouds due to their weak signal, which results in ambiguity differentiating between cloudy and clear-sky pixels.

[1]Earth System Science Interdisciplinary Center, University of Maryland, College Park, Maryland, USA.
[2]NASA Goddard Space Flight Center, Greenbelt, Maryland, USA.
[3]Science Systems and Applications, Inc., Lanham, Maryland, USA.
[4]Goddard Earth Science Technology and Research, Universities Space Research Association, Columbia, Maryland, USA.

Corresponding author: J. Lee, Earth System Science Inter disciplinary Center, University of Maryland, College Park, NASA Goddard Space Flight Center, Code 613, Greenbelt, MD 20771, USA. (jaehwa.lee@nasa.gov)

2169-897X/13/10.1002/jgrd.50806

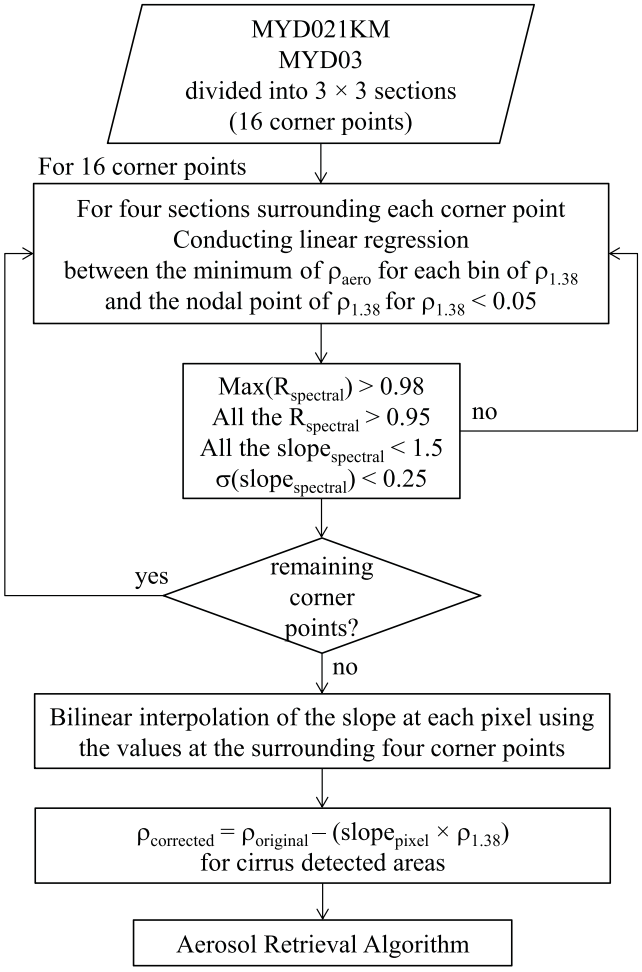

Figure 1. Cirrus correction process in the aerosol retrieval algorithm. R, σ, and ρ represent the Pearson correlation coefficient, standard deviation, and TOA reflectance, respectively. The subscripts "spectral" and "aero" are for wavelengths used in the aerosol retrieval algorithm (0.47, 0.55, 0.65, 0.86, 1.24, 1.63, and 2.12 μm).

[4] The MODIS sensors include a band centered near 1.38 μm, which is located within a strong water vapor absorption band, and so provides advantages for the detection of high clouds such as cirrus. When water vapor is abundant in the lower atmosphere, scattering at this wavelength will be attenuated by the water vapor, such that the TOA signal arises only from atmospheric constituents (aerosols and clouds) at high altitudes. Thus, the 1.38 μm band has been utilized in many cirrus-related investigations, including detection of thin cirrus clouds [*Gao et al*., 2002a; *Roskovensky and Liou*, 2003, 2005], deriving cirrus reflectance at visible wavelengths [*Gao et al*., 2002b; *Roskovensky et al*., 2004], and retrieving cirrus optical properties [*Dessler and Yang*, 2003; *Meyer et al*., 2004, 2007; *Meyer and Platnick*, 2010]. However, regions of low columnar water vapor or high-altitude aerosols can limit the applicability of the 1.38 μm band in detecting thin cirrus clouds.

[5] To achieve improved coverage and more accurate aerosol data products from satellites, a few studies have investigated methodologies for retrieving AOD under conditions of thin cirrus coverage. *Roskovensky and Liou* [2006] suggested a methodology for simultaneously retrieving optical properties of aerosols and thin cirrus clouds from MODIS. In their method, AOD, thin cirrus optical depth (COD), and ice crystal effective size were retrieved by first determining AOD using cirrus-corrected reflectance, which were calculated by removing the cirrus-only reflectance. The cirrus-only reflectance was derived from the correlation between the TOA reflectances in visible bands and 1.38 μm band [*Roskovensky et al*., 2004]. The AOD was then used in selecting the appropriate lookup table for cirrus optical properties in aerosol-present conditions. Finally, the COD and effective size were simultaneously retrieved by comparing the calculated and observed TOA reflectances at 0.65 or 0.86 μm and 1.64 μm. The retrieval also included an iterative process to resolve the impact of the retrieved cirrus effective size on the correlation between the visible and 1.38 μm reflectances, which were used in deriving cirrus-only reflectance, and thus, the cirrus-corrected reflectance and AOD. However, extensive evaluation of the cirrus-corrected AOD is still needed to assure the quality of the data on a larger scale, as the study only examined a few cases.

[6] *Pierce et al.* [2010] utilized Multiangle Imaging Spectroradiometer (MISR) data to retrieve cirrus-corrected AOD by adding two cirrus components to the MISR aerosol retrieval lookup table (which originally included only aerosol components), such that both AOD and COD could be retrieved during the inversion process. The inversion procedure of MISR was designed to assign the proportions for each aerosol/cirrus component that minimizes the difference between the observed and calculated TOA reflectances in both spectral and angular space. The extensive sensitivity study showed the sensitivity of the spectral and angular reflectances to the proportions of the aerosol/cirrus mixtures.

[7] In this study, we present a strategy for retrieving AOD under thin cirrus conditions from MODIS and compare the retrieved AOD with Aerosol Robotic Network (AERONET) observations [*Holben et al*., 1998] and Cloud-Aerosol Lidar with Orthogonal Polarization (CALIOP) retrievals [*Winker et al*., 2009]. The methodology for retrieving aerosol optical properties is somewhat similar to that of *Roskovensky and Liou* [2006], but we focus more on retrieving aerosol properties with a sophisticated aerosol retrieval algorithm [*Lee et al*., 2012] compared to the previous work, which focused on cirrus properties. In addition, we produce data at a high spatial resolution (1 km at nadir) to resolve the potential strong spatial variability of cirrus clouds and to conduct more accurate comparison with the CALIOP observations, which has 70 m beam width at the ground [*Kittaka et al*., 2011]. Detailed descriptions of the cirrus correction procedure, aerosol retrieval algorithm, collocation between MODIS and CALIOP, cirrus detection from MODIS, and sensitivity studies are provided in section 2. In section 3, a case study and evaluation of the cirrus-corrected AOD against AERONET and CALIOP data are given. Then, a summary and discussion of future work is presented in section 4.

2. Method

2.1. TOA Reflectance Correction for Thin Cirrus Signal

[8] To retrieve AOD under thin cirrus cover, we first correct the TOA reflectance for the thin cirrus signal. Since

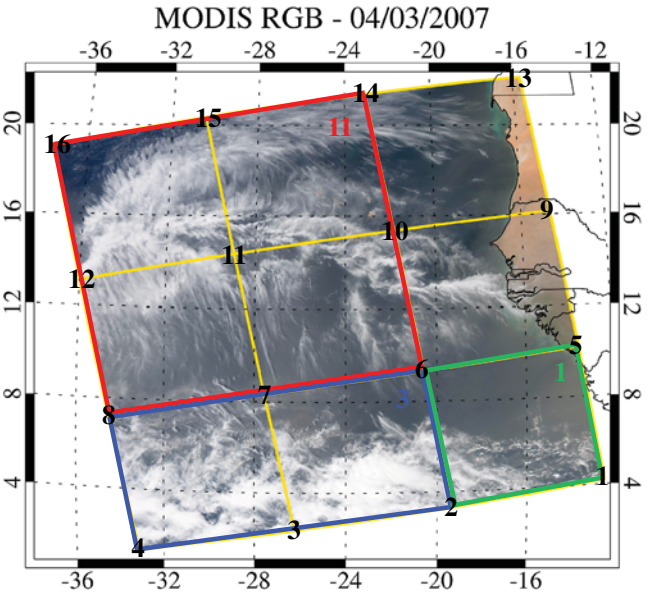

Figure 2. An example of MODIS-Aqua granule divided into 3 × 3 sections. Corresponding 16 corner points are also shown where the conversion factors are calculated using the data of the surrounding four sections. Areas used in calculating the conversion factors for numbers 1, 3, and 11 corner points are shown in green, blue, and red boxes, respectively. Data for the MODIS-Aqua granule collected at 15:05 UTC on 4 March 2007.

the correction requires cirrus-only reflectance to be subtracted from the observed TOA reflectance in each spectral band used in the aerosol retrieval algorithm, we adopt an empirical method to derive the cirrus-only reflectance from the TOA reflectance at 1.38 μm. The method was suggested by *Gao et al*. [2002b] and has been used in generating cirrus-signal-corrected satellite imagery [*Gao et al*., 2002b] and retrieving optical properties of cirrus clouds [*Meyer et al*., 2004, 2007]. The "cirrus reflectance" approach [*Meyer and Platnick*, 2010] takes advantage of the 1.38 μm band of MODIS located in the strong water vapor absorption band. Due to the strong absorption and a large portion of the water vapor residing in the lower troposphere, the TOA reflectance at 1.38 μm represents cirrus-only reflectance attenuated by water vapor absorption in and above the cirrus layer in cases of abundant columnar water vapor and absence of high clouds except for cirrus. Note that the molecular scattering at this wavelength is negligible due to low Rayleigh optical depth (<0.003) and its vertical dependence (i.e., concentrated toward the bottom of the atmosphere).

[9] In *Gao et al*. [1998], a linear relationship is assumed between the cirrus reflectance in visible bands and the 1.38 μm band,

$$\rho_c(\text{visible}) = a\rho_c(1.38\,\mu\text{m}), \tag{1}$$

where ρ_c is cirrus-only reflectance. Since, in reality, the measured reflectance at 1.38 μm is attenuated by in and above cirrus water vapor absorption, the slope parameter includes the effect of water vapor absorption as follows:

$$\rho_c(\text{visible}) = \Gamma\rho(1.38\,\mu\text{m}), \tag{2}$$

where Γ is aT_w and T_w is two-way transmittance for water vapor in 1.38 μm band. The conversion factor Γ can then be derived by calculating the slope of the linear regression line between binned TOA reflectance at 1.38 μm and the minimum reflectance in the visible band in each specific bin of the reflectance at 1.38 μm, in a "scatterplot" technique [*Gao et al*., 2002b]. The reason for selecting the minimum reflectance in the visible band is that TOA reflectance here represents the combined signal of air molecules, surface reflectance, aerosols, and low clouds, as well as cirrus clouds, in contrast to the 1.38 μm reflectance which arises in these cases only from high clouds such as cirrus. By definition, the procedure was designed to find dark and homogeneous underlying pixels with varying cirrus reflectance to derive the correlation between cirrus reflectance in 1.38 μm and the visible bands. If there are a sufficient number of such pixels, the two variables show high correlation, and cirrus reflectance in the visible band can be derived. As multiple points are required to perform this regression, the method requires data over an area rather than a single pixel.

[10] Figure 1 shows the cirrus correction process in the aerosol retrieval algorithm. In this study, a modified version of the over-ocean algorithm introduced by *Lee et al*. [2012] is used, which requires TOA reflectances at 0.47, 0.55, 0.65, 0.86, 1.24, 1.63, and 2.12 μm (hereafter, "aerosol bands"). The process first divides a MODIS granule into nine sections (3 × 3 grid with 16 corner points) with equal distance in longitude and latitude and conducts the scatterplot technique for each aerosol band at each corner point using the surrounding four sections (cf. Figures 2 and 3). When calculating the conversion factor Γ, the minimum reflectance in each aerosol band is calculated for every 0.005 interval of 1.38 μm reflectance in the range from 0.002 to 0.052. In this application, we correct for cirrus reflectance up to 0.05. For brighter scenes, as a result of factors such as multiple scattering, the linear assumption in calculating cirrus-corrected TOA reflectance (i.e., simple subtraction of cirrus reflectance from the measured TOA reflectance) may be less appropriate.

[11] Then, a set of tests on the Pearson correlation coefficient and slope, as shown in Figure 1, are conducted to check the validity of the correlation of cirrus signals between the two wavelengths. When the scene passes the test, the slope is stored to be used in correcting the cirrus signal. After processing all the 16 corner points, the conversion factors at each MODIS pixel are calculated for each section by using bilinear interpolation of the conversion factors at the four corner points surrounding the section, but only if all the four values are valid. The four-value-validity test is to exclude sections where the correction is ambiguous (e.g., insufficient cirrus coverage or weak relationship between 1.38 μm and aerosol band reflectance). For 1384 granules processed in this investigation, out of all the sections with at least one valid conversion factor, 53% of those passed the test. The TOA reflectance for the aerosol bands is then corrected by subtracting the cirrus-only reflectance from the original TOA reflectance and passed into the aerosol retrieval algorithm to retrieve cirrus-corrected aerosol optical properties.

[12] Figure 2 shows an example MODIS granule divided into 3 × 3 sections with the corresponding 16 corner points where the conversion factors are calculated. Since the cirrus

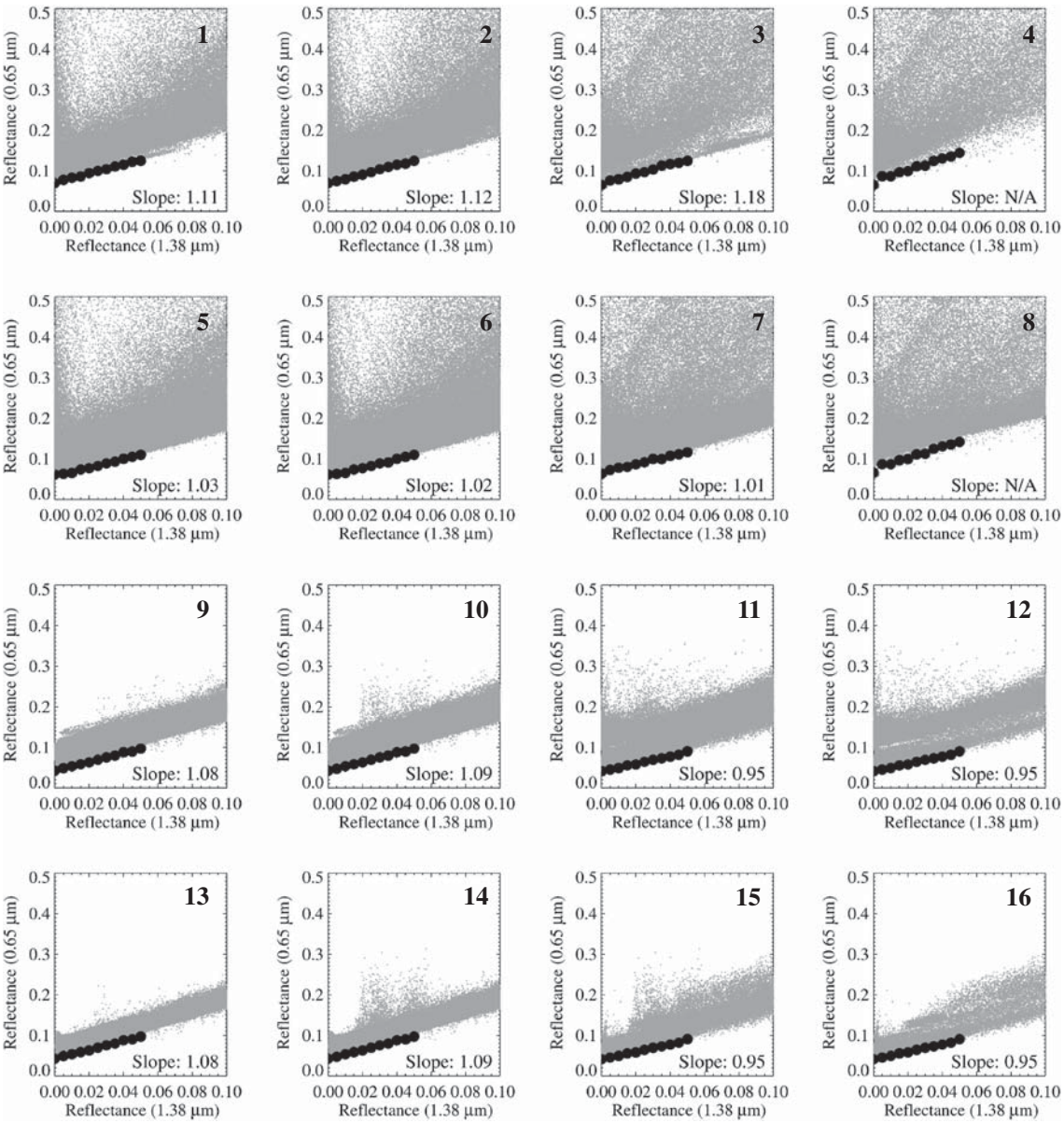

Figure 3. Scatterplots between TOA reflectance at 1.38 and 1.24 μm at the 16 corner points of the MODIS granule shown in Figure 2. Black circles are the minimum values of 1.24 μm reflectance in each bin of 1.38 μm reflectance, in bins of size 0.005 ranging from 0.002 to 0.052. This plot corresponds to the case study shown in Figure 8.

correction procedure is applied on a granule basis (no stitching between granules), the available number of sections is different for different locations. For example, only one section is available at corner point numbers 1, 4, 13, and 16, two sections at numbers 2, 3, 5, 9, 8, 12, 14, and 15, and all four sections at numbers 6, 7, 10, and 11. The corresponding scatterplot shown in Figure 3 indicates a strong linear relationship between the two wavelengths. The difference in the conversion factor varying from 0.95 to 1.18 is mainly due to the spatial variability of water vapor and cirrus optical properties, cirrus absorption in particular. Although a previous study suggested the linear assumption is valid between 0.4 and 1.0 μm [*Gao et al.*, 1998], we find that it can be extended to even longer wavelengths (1.63 and 2.12 μm) for optically thin cases (Figure 4). However, the nonlinearity at higher reflectances limits the applicability of the method for longer wavelengths to optically thin cases. It should be noted that by thorough checking of each scatterplot generated in this investigation, no obvious change is found in the slope with respect to 1.38 μm reflectance less than 0.05. This allows us to use linear regression approach for optically thin cases.

[13] By doing so, the approach incorporates the effect of in and above cirrus water vapor absorption at 1.38 μm when converting the cirrus reflectance at 1.38 μm into other wavelength bands. The method also accounts for the cirrus spectral optical properties (most importantly cirrus absorption), since the slope is calculated for each wavelength. However, there are inherent limitations caused by using a broad spatial area in calculating the correlation. The slope calculated via the scatterplot technique assumes homogeneous microphysical

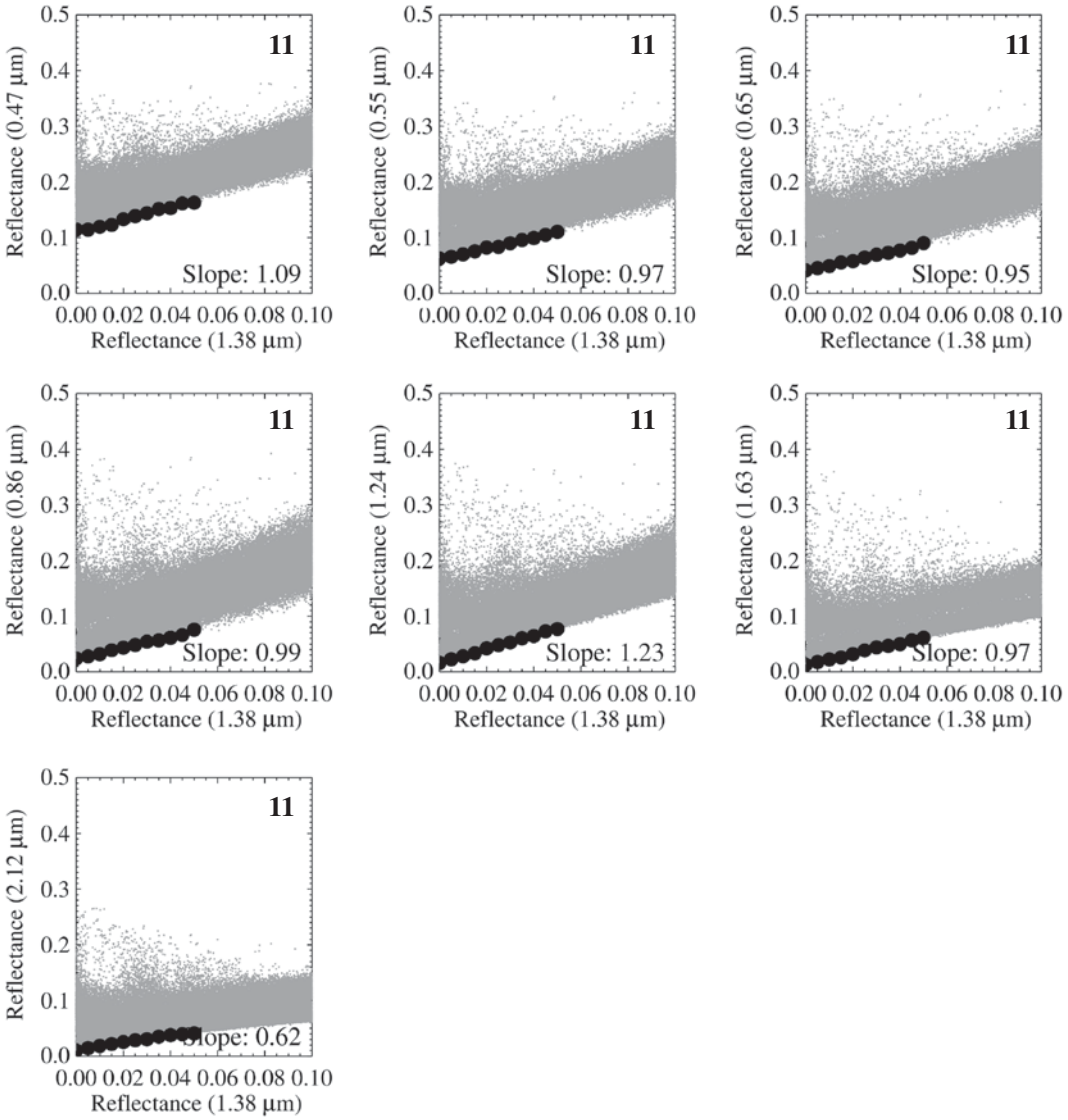

Figure 4. Spectral scatterplots between TOA reflectance at 1.38 μm and aerosol bands at number 11 corner point where cirrus clouds are observed.

properties (size and shape) and water vapor absorption in and above cirrus clouds in a wide area (~777 × 677 km), since a fixed value is derived for the entire area. Moreover, it is inevitable that errors caused from the difference in spatial distribution of air mass and atmospheric phase function between the two wavelengths will propagate into the correction. Although we use nine sections for a MODIS granule to calculate the conversion factor, reducing the size of the target area is expected to mitigate the error resulting from using the areal approach. However, reducing the sampling area would also decrease applicability of the method by reducing the possibility of finding a valid conversion factor. Further study is needed to optimize the sample size for the best combination of accuracy and coverage.

2.2. Aerosol Retrieval Algorithm Over Ocean

[14] *Lee et al.* [2012] introduced an algorithm to retrieve aerosol optical properties over ocean from MODIS with an improved aerosol microphysical model suite. Originally, the algorithm was developed to test impacts of new aerosol models on the retrieval quality compared to the MODIS Collection 5 aerosol products. Thus, it was designed similarly to the operational MODIS algorithm [*Remer et al.*, 2005] except for the aerosol models and a minor change to the wavelength bands used in different AOD conditions, i.e., 0.65, 0.86, 1.24, 1.63, 2.12 μm for AOD ≤ 0.15 and all the seven aerosol bands including 0.47 and 0.55 μm for AOD > 0.15. The use of longer wavelengths for low-AOD conditions is to minimize errors caused from ocean surface reflectance, which increase with decreasing wavelengths. The algorithm retrieves AOD at 0.55 μm and aerosol model by minimizing the difference between calculated and observed spectral reflectance (lookup table approach) using 23 aerosol models. It also derives fine mode fraction (FMF) of AOD at 0.55 μm and single-scattering albedo (SSA) at 0.44 μm, as the aerosol models were created with respect to these two variables.

[15] The algorithm originally took the cloud-screened and gas-corrected Level 2 spectral reflectance data in 10 × 10 km resolution as input data ("MYD04_L2"), but we modified the algorithm to use Level 1B reflectance data ("MYD021KM"),

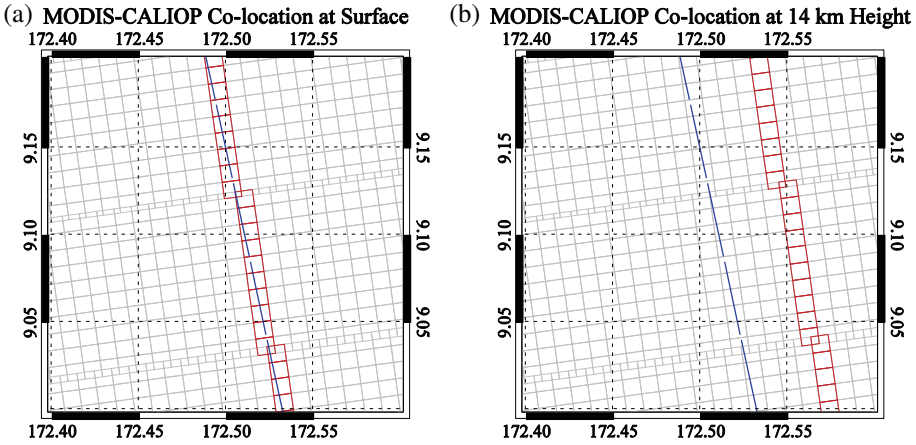

Figure 5. An example of collocated MODIS and CALIOP footprints at (a) surface and (b) 14 km height. Blue lines represent CALIOP foot prints in 5 km resolution, and red boxes collocated MODIS pixels in 1 km pixel resolution. There are at maximum five collocated MODIS pixels corresponding to a single CALIOP footprint.

which have 1 km pixel resolution at nadir, to retrieve aerosol properties at high spatial resolution. It is useful to use high-resolution data due to the potential strong spatial variability of cirrus clouds. A new lookup table was produced using 6SV radiative transfer code [*Kotchenova et al.*, 2006; *Kotchenova and Vermote*, 2007] to include the polarization effect since the original table were generated using the scalar discrete ordinates radiative transfer code [*Stamnes et al.*, 1988; *Mayer and Kylling*, 2005]. The MODIS Collection 5 gas correction and cloud-screening procedures [*Remer et al.*, 2006] were also implemented.

[16] The cloud-screening procedure detects thin cirrus clouds with $\rho_{1.38}/\rho_{1.24} > 0.3$ or $[0.10 \le \rho_{1.38}/\rho_{1.24} \le 0.30$ and $\rho_{1.38} > 0.03$ and $\rho_{0.66} > 1.5\rho_{\mathrm{ray},0.65}]$ [*Remer et al.*, 2005], where ρ represents TOA reflectance with subscripts representing wavelengths in micrometer, and ρ_{ray} is the reflectance calculated for aerosol-free conditions (i.e., Rayleigh atmosphere). The spatial variability test [*Martins et al.*, 2002] and thick homogeneous cloud test ($\rho_{0.47} > 0.40$) [*Remer et al.*, 2005] were also implemented into the retrieval process. The retrieval target areas are confined to "Moderate or Continental Ocean" and "Deep Ocean" as assigned by the MODIS land/sea mask from the geolocation product ("MYD03"). "Shallow Ocean" (ocean < 5 km from coast or 50 m deep) is not included because of possible errors caused from ocean turbidity and bottom reflection.

[17] We generated two different cirrus-corrected AOD data sets to compare with the cirrus-uncorrected data set. The first data set was created by applying the cirrus correction procedure after the cloud screening, such that data coverage is the same as the cirrus-uncorrected data set. For the second data set, the cirrus correction procedure is applied before the cloud screening, such that the cirrus-corrected area is not masked out by the cirrus screening procedure. As a result, there is some "recovered" area in the second data set, which is screened out in the uncorrected data set.

2.3. Collocation Between MODIS and CALIOP

[18] Evaluation of the cirrus-corrected AOD is a challenge since there are few accurate data sources under cloudy conditions. CALIOP, however, is able to provide aerosol data under transparent cirrus conditions, despite the known systematic bias of AOD due to the assumed lidar ratio [*Oo and Holz*, 2011; *Sayer et al.*, 2012; *Schuster et al.*, 2012]. For our comparisons, we utilize the 5 km aerosol and cloud layer products ("CAL_LID_L2_05km[AC]Lay-Prov-V3-01") to evaluate our MODIS 1 km cirrus-corrected AOD and AOD correction magnitude (defined as the difference between AODs without cirrus correction and with cirrus correction). The correction magnitude mainly depends on the cirrus reflectance, and thus COD.

[19] To compare data from the two different satellites, the data must be collocated in space and time. The collocation procedure is designed to find the closest MODIS pixels within 700 m of the five subpoints of a CALIOP footprint to account for the difference in the spatial resolution between

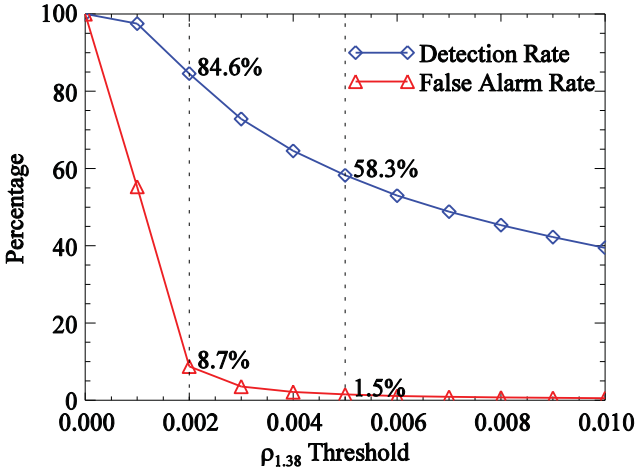

Figure 6. Cirrus detection rate and false alarm rate of MODIS with respect to $\rho_{1.38}$ threshold values in reference to the cirrus detection from CALIOP over the eastern tropics (60°E–180°E, 15°S–15°N) for the period from 1 March 2007 to 31 May 2007. The total numbers of data points for the cirrus-detected and clear cases determined by CALIOP are 105,548 and 54,243, respectively.

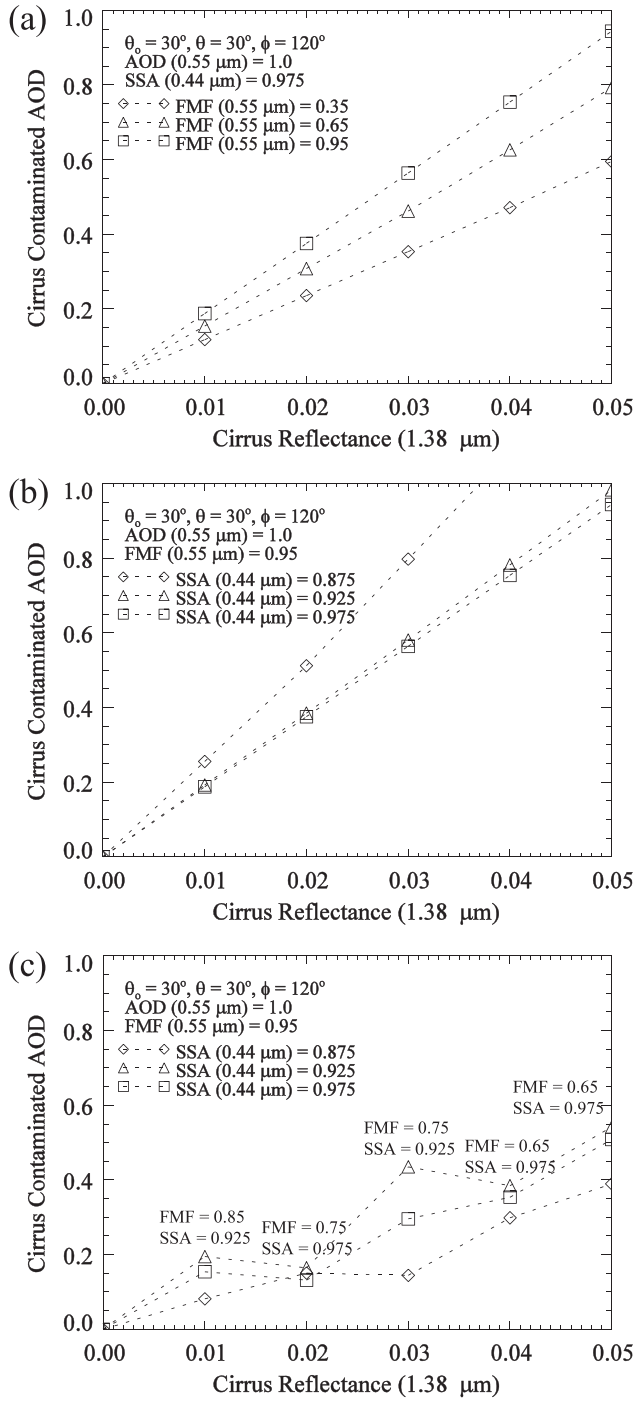

Figure 7. Cirrus contamination magnitude in AOD with respect to cirrus reflectance at 1.38 μm for (a, b) fixed aerosol models and (c) real inversion. Three different aerosol models superimposed on the plots do not change with respect to the cirrus reflectance for the fixed aerosol model cases, while the aerosol models represent initial candidates and can change during the inversion process for the real inversion case. Aerosol models used at each nodal point are shown for the case of SSA (0.44 μm) = 0.925.

the two data sets, i.e., 5 km for CALIOP and 1 km for MODIS. By doing so, a maximum of five MODIS pixels are selected that correspond to a single CALIOP footprint. For the AOD comparison, collocation can be done using the original geolocation data from CALIOP and MODIS assuming an aerosol layer near the surface. However, when comparing cirrus signals at high altitudes between the two instruments, i.e., AOD correction magnitude from MODIS and COD from CALIOP, the parallax effect should be taken into account since the MODIS-CALIOP collocation track is off-nadir of the MODIS swath. To this end, we calculate new MODIS latitude and longitude values at cirrus heights by solving a simple trigonometric function assuming a plane-parallel atmosphere which incorporates the cirrus layer heights from CALIOP and viewing and inclination angles of MODIS. The same collocation procedure as above is then applied using the new (cirrus level) geolocation data. The plane-parallel assumption has negligible effect on the results because of the small viewing zenith angles of MODIS at the CALIOP observation track ($< 20°$) and large MODIS pixel size compared to the narrow beam width of CALIOP. Figure 5 shows an example of collocated MODIS and CALIOP footprints at the surface and at an altitude of 14 km, showing a shift of about four MODIS pixels between the two height levels. Note that in the real case, we utilize the observed cirrus layer top heights from CALIOP.

2.4. Thin Cirrus Detection Using 1.38 μm Band of MODIS

[20] The 1.38 μm reflectance is not a perfect indicator of the presence of cirrus clouds and may be contaminated by underlying water clouds, aerosols, and even the surface. So before applying the cirrus correction procedure, a threshold must be determined to represent the thin cirrus detection limits of the 1.38 μm band. Selecting too low a threshold can cause overcorrection, while a threshold that is too high will cause undercorrection.

[21] To determine an appropriate threshold, we compared the cirrus detection performance of the 1.38 μm band of MODIS with CALIOP feature classification flag. Figure 6 shows the cirrus detection rate (both instruments detect cirrus) and false alarm rate (only MODIS detects cirrus) of MODIS as a function of the 1.38 μm reflectance threshold. The comparison was conducted using data from March to May 2007 over the region from 60°E to 180°E and 15°S to 15°N (hereafter the "eastern tropics"), where cirrus clouds are frequently observed [*Sassen et al.*, 2008]. For this figure, thresholds varying from 0.0 to 0.1 were applied to the MODIS 1.38 μm reflectance where reflectances greater than the threshold were assumed to be cirrus clouds. For CALIOP, the feature classification flags were used and cirrus clouds were assumed to satisfy all of the following conditions: "feature type," cloud; "feature type QA," high; "ice/water phase," randomly oriented ice or horizontally oriented ice; "phase QA," high; "feature subtype," cirrus (transparent).

[22] Meanwhile, clear-sky conditions were defined when neither ice nor water clouds were detected by CALIOP. Although water clouds are expected to increase the false alarm rate due to enhanced 1.38 μm reflectance for specific conditions, we excluded the data since those scenes are effectively detected and screened out by the cloud-screening process of the MODIS aerosol retrieval algorithm [*Martins et al.*, 2002]. The aforementioned collocation technique was used in this application as well. As a result, we decided

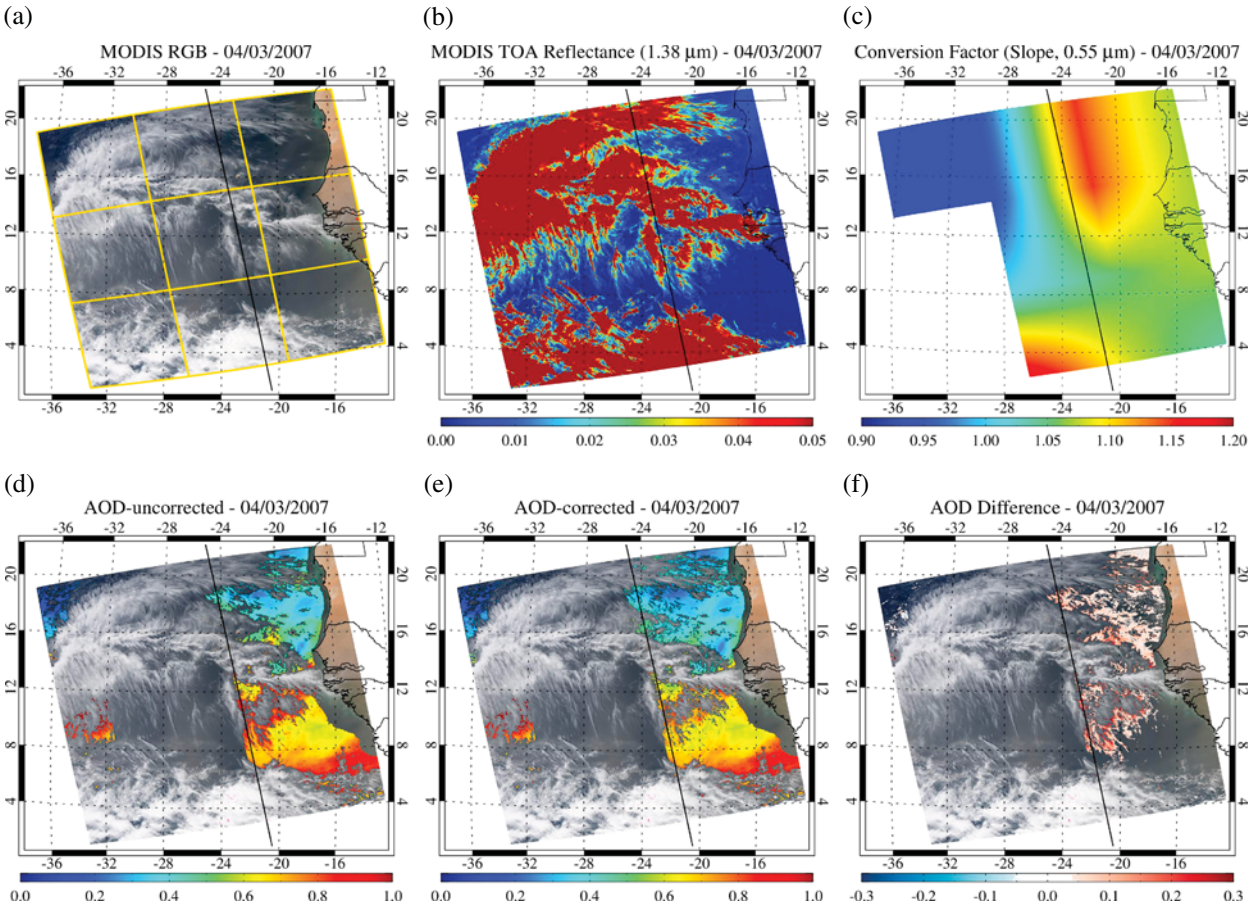

Figure 8. (a) MODIS RGB image, (b) TOA reflectance at 1.38 μm, (c) conversion factors at 0.55 μm, (d) AOD without cirrus correction, (e) AOD with cirrus correction, and (f) AOD difference between the two (uncorrected and corrected). Figures 8d–8f are calculated using the developed algorithm in this investigation. Data for the MODIS granule collected at 15:05 UTC on 4 March 2007. The black line represents the CALIOP observation track.

to use a threshold of 0.002, which shows a detection rate of 84.6% and a false alarm rate of only 8.7%. The false alarm rate is somewhat high, but it steeply decreases with the threshold, and reflectance change of order 0.001 will result in negligible error compared to the errors caused from the cirrus correction method itself. Note that a false alarm rate of only 1.5% is observed for the threshold of 0.005. The reflectance difference of 0.003 corresponds to an AOD difference of about 0.03 regardless of aerosol model in the case of solar zenith angle = 30°, viewing zenith angle = 30°, and relative azimuth angle = 90°, and the magnitude varies with AOD and observation geometry. It should be noted that over this area, scenes with cirrus clouds occur about twice as frequently as clear-sky scenes along the CALIOP observation track, showing the necessity of a cirrus correction algorithm for better accuracy and coverage of aerosol products in this region.

2.5. Sensitivities of AOD to Cirrus Reflectance

[23] Sensitivity studies were carried out to show the effect of cirrus contamination on the retrieved AOD. Figure 7 shows the cirrus-contaminated AOD with respect to cirrus reflectance at 1.38 μm. The spectral conversion factors used are adopted from the case study shown in Figure 4. The AOD sensitivities are calculated using 0.86 μm, which is the reference wavelength used in the aerosol retrieval algorithm. For the fixed aerosol model cases (Figures 7a and 7b), cirrus contamination in AOD increases with increasing cirrus reflectance, decreasing aerosol size (increasing FMF), and increasing absorption (decreasing SSA). We found that the magnitude of cirrus contamination generally (but not always) increases with increasing AOD and decreasing air mass (not shown).

[24] A more realistic case is shown in Figure 7c, which is calculated using the real inversion procedure used in the aerosol retrieval algorithm and spectral reflectances for the three different initial aerosol models with three different SSA and fixed FMF. Although the cirrus contamination shows in general an increasing tendency with cirrus reflectance, the overall magnitude is significantly reduced compared to the fixed aerosol model cases. The aerosol retrieval algorithm tends to choose larger aerosol models as cirrus contamination increases, but nothing similar is found in SSA. It should be noted that different aerosol model selection sometimes leads to a lower AOD at higher cirrus reflectance, which was not observed in the fixed aerosol model cases. In actual use, the cirrus correction magnitude is expected to be up to 0.8 in AOD for cirrus reflectance of 0.05 depending on viewing geometry, AOD, and aerosol model.

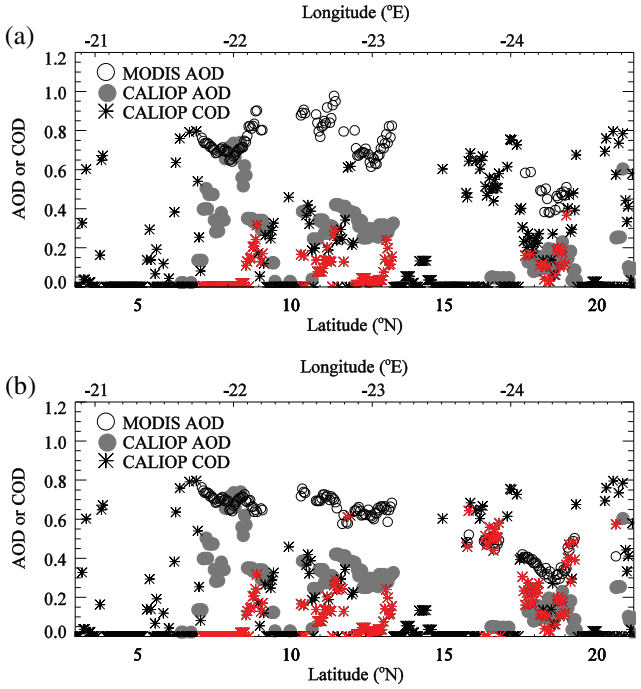

Figure 9. Comparison between (a) CALIOP AOD and MODIS AOD-uncorrected and (b) CALIOP AOD and MODIS AOD-corrected for the case study shown in Figure 8. Only CALIOP COD smaller than 0.8 are shown. The CALIOP COD data paired with the MODIS data are shown in red.

3. Results

3.1. Case Study

[25] Figure 8 shows a case study off of the coast of Africa on 4 March 2007. On this day, a moderate aerosol event is observed with AOD ranging from 0.3 to 0.9, and some areas are under cirrus clouds. AOD data were not retrieved over the center portion of the image due to sun glint. Mixed dust and smoke aerosols are common in this region at this time of year [e.g., *Eck et al.*, 2010]. The AERONET midvisible Ångström exponent for sites in this region on this day was generally less than 0.5 (not shown), suggesting an optical dominance of mineral dust aerosols, although MODIS fire counts and visible images support the presence of some smoke. The corresponding scatterplots (Figures 3 and 4) show strong correlations between TOA reflectance at 1.38 μm and the aerosol bands, allowing the scene to be corrected for thin cirrus contamination. The AOD without the cirrus correction procedure (hereafter, AOD-uncorrected) shows apparent imprints of thin cirrus contamination around 8°N to 12°N near the CALIOP track where the 1.38 μm reflectances show enhancement, while the cirrus-corrected AOD (hereafter, AOD-corrected) shows reduced contamination and spatial variability over the same areas. It should be noted that the cirrus correction procedure not only reduces the contamination but also recovers some areas (16°N–18°N, 20°W–24°W) which were screened out by the cloud-screening procedure. In this case, the magnitude of the AOD correction is as large as 0.35 and shows the strong impact of thin cirrus contamination on AOD.

[26] To further analyze the results in a quantitative way, we show, in Figures 9 and 10, the comparison between CALIOP AOD at 0.532 μm and MODIS AOD at 0.55 μm with and without the cirrus correction, and between CALIOP COD at 0.532 μm and MODIS AOD correction magnitude (AOD-uncorrected and AOD-corrected) along the CALIOP observation track. Although systematic low biases are documented in CALIOP AOD, noticeable differences are seen between the two AOD data sets when compared. The increasing tendency of the AOD-uncorrected data set with latitude around 9°N is reversed after the cirrus correction, resulting in a similar tendency to the CALIOP AOD. The increasing tendency in the AOD-uncorrected data seems to be correlated with the COD from CALIOP, which represents cirrus contamination in the AOD data. A similar pattern is shown in the data between 10°N and 14°N where the cirrus correction reduces the AOD values and consequently, the correlation between AOD and COD. An area that was previously cloud screened but recovered due to the cirrus correction can also be seen near 17°N.

[27] A comparison of CALIOP COD and MODIS AOD correction magnitude is shown in Figure 10. There we find a high correlation between the two parameters with the Pearson correlation coefficient of 0.89 and near one-to-one slope (0.94), suggesting a high degree of skill in the cirrus corrections. Note that the AOD correction magnitude and COD are analogous in that both parameters are column-integrated amounts derived from the cirrus reflectance, although a one-to-one AOD-COD relationship is not necessarily expected in the general case, due to the difference between scattering properties of aerosol and cirrus. More detailed description on the correlation between the two variables will be given in section 3.3.2.

3.2. Comparisons Against AERONET Observations

[28] Figure 11 compares cirrus-uncorrected and corrected AOD data sets with AERONET observations at Nauru in the equatorial Pacific (0.5°S, 166.9°E) for the period from 1

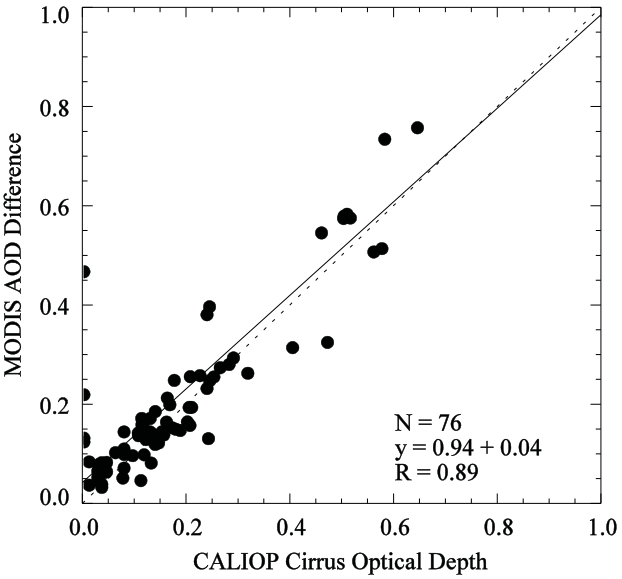

Figure 10. Scatterplot between CALIOP COD and MODIS AOD correction magnitude (AOD-uncorrected and AOD-corrected) for the case study shown in Figure 8. Data for the recovered area are also shown, of which data cluster is shown on CALIOP COD > 0.4.

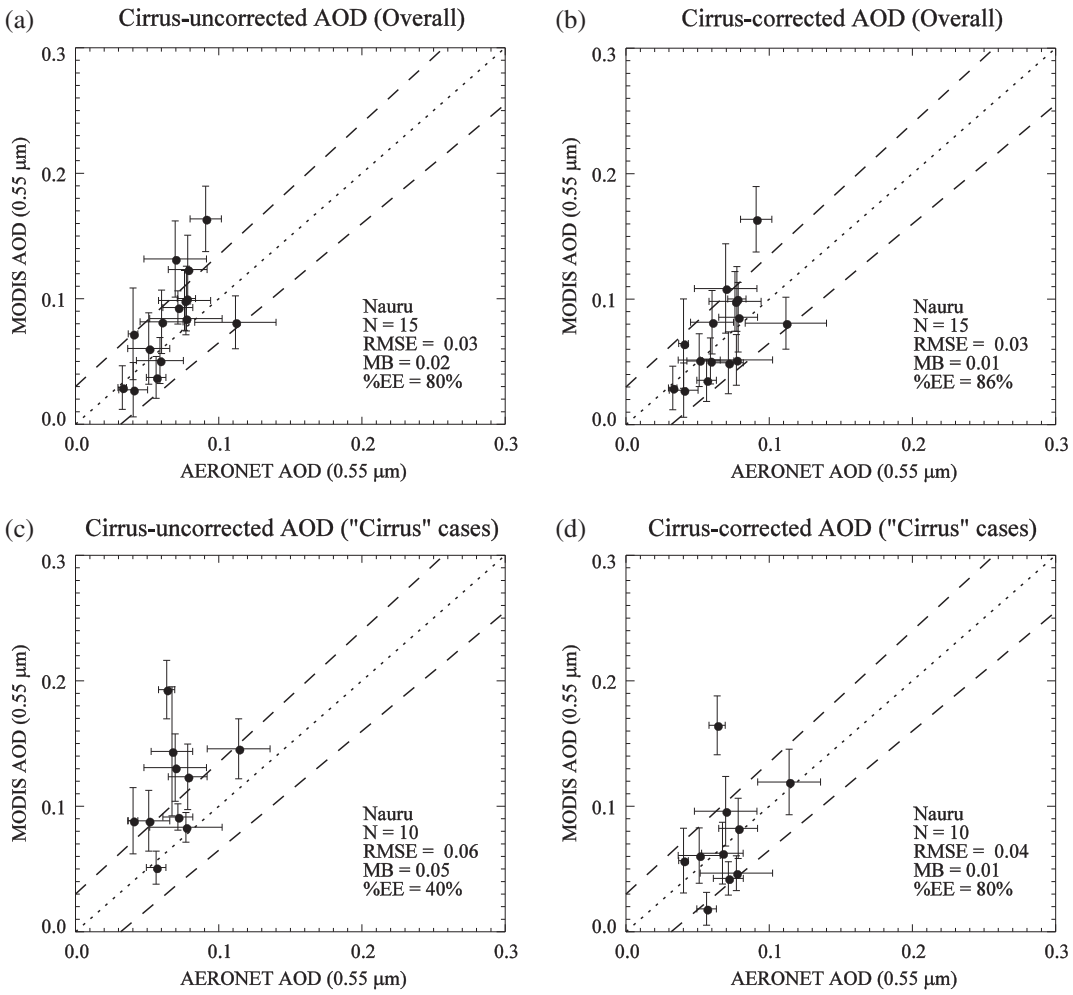

Figure 11. Comparisons of MODIS AODs against AERONET observations at Nauru site for the cases of (a) AOD-uncorrected overall data, (b) AOD-corrected overall data, (c) AOD-uncorrected cirrus cases, and (d) AOD-corrected cirrus cases. The solid, dotted, and dashed lines represent the linear least square regression, one-to-one, and MODIS expected error (EE) lines, which is defined as $\pm(0.03 + 0.05 \times \mathrm{AOD})$, respectively. The statistics shown are the number of data points (N), the Pearson correlation coefficient (R), root-mean-squared error (RMSE), mean bias (MB), and the percentage within expected error (%EE).

March to 31 May 2007. For this investigation, cloud-screened and quality-assured Level 2 AERONET data are used, and the collocation between the two data sets was made within 25 km in space and 2 h in time. Typically, a limit of 30 min is used with AERONET comparisons, but this was expanded to increase sampling as we compare data under cirrus condition. Note that only limited matchups were found within 30 min window. However, because of its location in remote ocean far from source regions, spatiotemporal variability of AOD around the Nauru site is expected to be weak.

[29] The comparison reveals that the cirrus correction procedure improves the data quality as shown by an increased percentage of data within the expected error of the operational MODIS product, $\pm(0.03 + 0.05 \times \mathrm{AOD})$, from 40% to 80% for cirrus-corrected areas (hereafter, "cirrus" cases) and from 80% to 86% for overall collocated data regardless of the application of the cirrus correction procedure. The reduction of positive mean biases is obvious (0.05 to 0.01 for the cirrus case, 0.02 to 0.01 for overall data) as the cirrus correction generally results in reduced AOD.

[30] Recent findings suggested possible thin cirrus contamination in the Level 2 AERONET data set [*Huang et al.*, 2011, 2012]. However, the susceptibility percentage was generally less than 5–10% according to matchup data sets (Micro-Pulse Lidar network, CALIOP). Given the fact that AERONET can be cirrus-contaminated only by very thin stable cirrus [*Smirnov et al.*, 2000] and the cirrus correction is usually applied to the edge of cirrus system where spatial gradient of COD is large, the cirrus contamination in the AERONET data set is expected to be negligible. In addition, the low AOD at Nauru site is a favorable condition for AERONET to detect temporally varying cirrus signals. The limited number of samples in the collocated data set between AERONET and MODIS within 30 min criterion further supports this argument.

3.3. Comparisons Against CALIOP Retrievals

[31] Here, we present comparison results of MODIS data sets with CALIOP aerosol and cloud products over the eastern tropics for a 3 month period ranging from March to

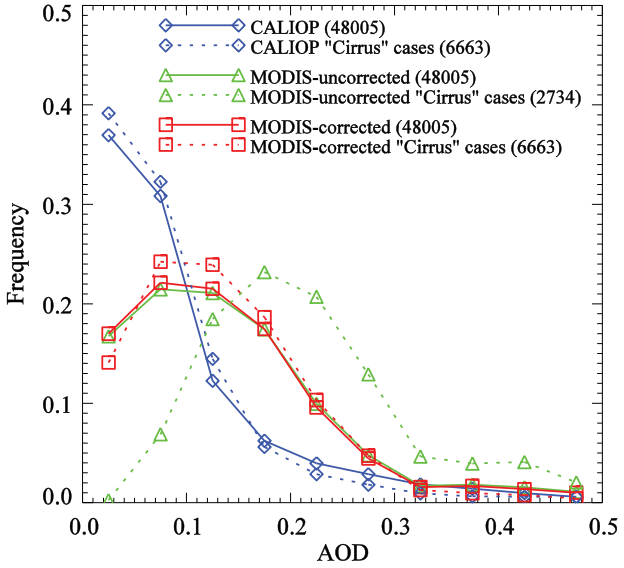

Figure 12. Normalized frequency distribution of CALIOP AOD and MODIS AOD data sets for different conditions over the eastern tropics, for the period from 1 March 2007 to 31 May 2007. The normalized frequencies are calculated in an interval of 0.05 in AOD.

May 2007. The eastern tropics was found to be the region of most frequent cirrus occurrence [*Sassen et al*., 2008], which helps to increase the sampling size to be compared. For AOD data from MODIS and CALIOP, we conducted frequency distribution analysis instead of direct comparisons since CALIOP AOD shows relatively poor accuracy compared with data sources that have conventionally been used (e.g., AERONET) [*Kittaka et al*., 2011; *Oo and Holz*, 2011]. A long-term comparison of the MODIS AOD correction magnitude with the CALIOP COD is also presented, which was revealed to have high correlation from the case study.

3.3.1. AOD

[32] Figure 12 compares the frequency distribution of AOD data from different sources and conditions. While the CALIOP AOD shows a significantly higher frequency in the low-AOD regime (AOD < 0.1) compared to the MODIS counterpart, the MODIS "overall" data (i.e., including cirrus-uncorrected data) show a slight increase of frequency in the high-AOD regime (AOD > 0.2) and decrease in the low-AOD regime (AOD < 0.2) as compared to the cirrus-corrected counterpart. This implies cirrus contamination in the cirrus-uncorrected data set. This tendency is magnified by only considering the cirrus cases and shows a significant shift of the frequency distribution to the higher-AOD regime when the cirrus signals are not properly corrected. It should be noted that the cirrus-corrected AOD shows a similar frequency distribution with the overall cases, which mainly include clear-sky data.

[33] Figure 13 shows the spatial distributions of seasonal mean AOD from different data sets and the difference between AOD-uncorrected and AOD-corrected data sets. The seasonal mean AOD in this region shows low values (~0.1) except for off the coast of southern India (~0.4). Both the corrected and uncorrected data show a similar seasonal pattern in the region, but the uncorrected AOD, in general, is higher than the corrected AOD by up to 0.02. In some smaller areas, the uncorrected AOD data is lower than the corrected data due to difference in sampling as the cirrus correction recovers some data previously lost due to cloud filtering. Note that the cirrus correction procedure generally reduces the AOD due to the lower TOA reflectance except when a different aerosol model is used during the retrieval process. The data for cirrus cases also show similar pattern with the overall cases. The observed differences are mainly due to a reduction in sample size.

3.3.2. AOD Correction Magnitude

[34] Figure 14 shows scatter density plots between CALIOP COD and the magnitude of MODIS AOD correction. The high correlation (R = 0.89) between the two parameters implies low random error in the cirrus correction procedure. Remarkably, the correlation is much higher than the AOD comparison [*Kittaka et al*., 2011; *Oo and Holz*, 2011] despite the difference in the sources of signals (aerosol versus cirrus). This is likely due to the fixed CALIOP lidar ratio for cirrus (25 ± 10 sr) (http://www-calipso.larc.nasa.gov/resources/calipso_users_guide/data_summaries/layer/#dq)

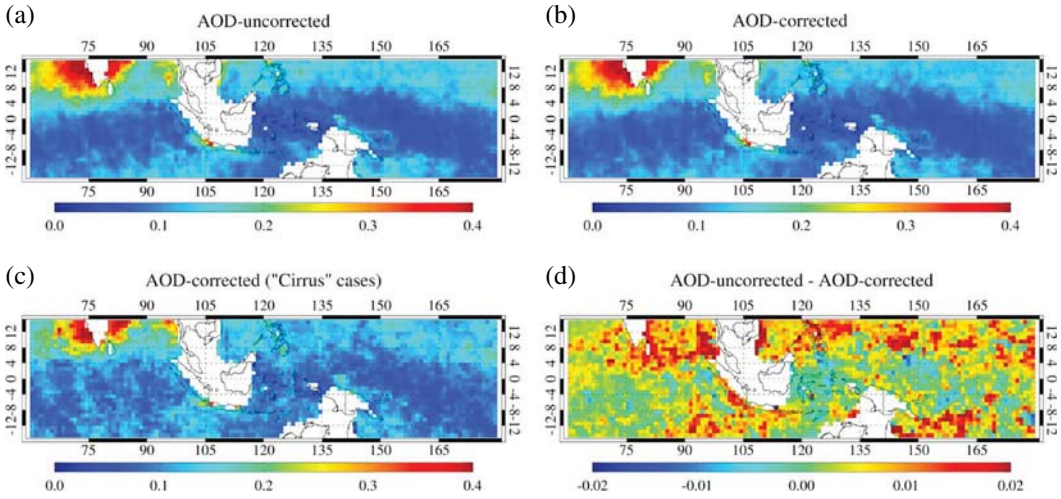

Figure 13. Spatial distribution of seasonal mean AOD for (a) AOD-uncorrected, (b) AOD-corrected, (c) AOD-corrected for cirrus cases, and (d) seasonal mean AOD difference (uncorrected and corrected) over the eastern tropics for the period from 1 March 2007 to 31 May 2007.

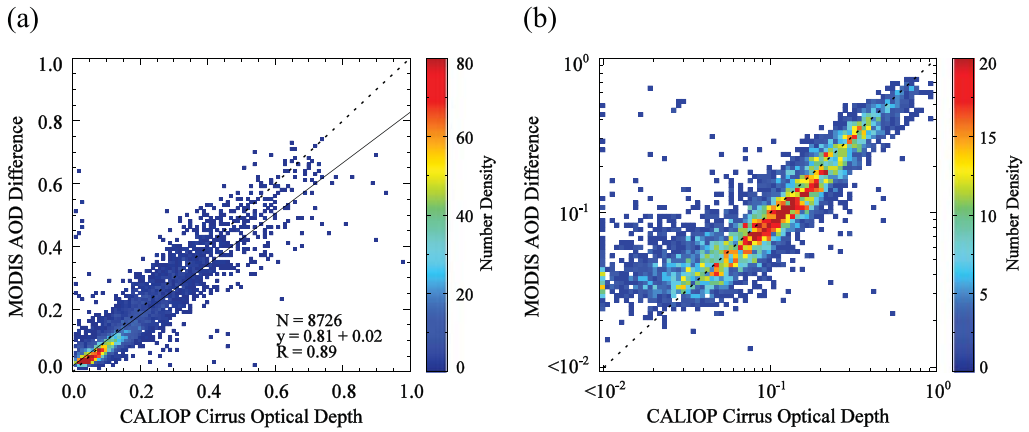

Figure 14. Scatter density plots between CALIOP COD and MODIS AOD correction magnitude including the recovered areas over the eastern tropics for the period from 1 March 2007 to 31 May 2007. Plots are on a (a) linear scale and (b) log-log scale. The solid and dotted lines represent the linear least squares regression and one-to-one lines, respectively.

and more accurate laser beam signals at high altitudes [*Kim et al*., 2008; *Mamouri et al*., 2009; *Wu et al*., 2011]. In addition, confining the data set to only thin cirrus clouds may reduce errors caused by varying cirrus optical properties (ice crystal shape and size), which would result in varying lidar ratios.

[35] The reason for the ~20% (regression slope of 0.81) difference between the two parameters is that marine aerosols have lidar ratios of 25–35 [*Sayer et al*., 2012, and references therein], which are 0–40% higher than that assumed for cirrus in the CALIOP retrievals. Marine aerosols are the dominant aerosol type over much of the study area for low-AOD cases (AOD < ~0.2). An increasing tendency of the slope with COD is also shown (slope approaches to one) likely due to finer mode aerosol model selection after correction (cf. Figure 7c), which results in a lower AOD compared to the fixed aerosol model selection, and thus increasing the correction magnitude. Note that given TOA reflectance and aerosol absorptivity, retrieved AOD is lower for fine mode cases than that of coarse mode due to stronger backscattering fraction of small particles.

4. Conclusions and Potential Future Studies

[36] A strategy for retrieving AOD over ocean under conditions of thin cirrus cloud coverage from MODIS has been presented and evaluated through comparison with AERONET observations and CALIOP aerosol and cloud products. The evaluation was conducted over the eastern tropics for the 3 month period from March to May 2007. To retrieve cirrus-corrected aerosol optical properties, the over-ocean aerosol retrieval algorithm adopted the scatterplot technique [*Gao et al*., 2002b], which derives the cirrus reflectance in each aerosol band using the correlations between reflectance at 1.38 μm and the aerosol bands at synoptic scales. The cirrus reflectance was then used in calculating cirrus-corrected TOA reflectance as required in the aerosol retrieval algorithm.

[37] The case study for a mixed dust/smoke aerosol event showed that the cirrus correction algorithm significantly decreased the (positive) cirrus contamination in AOD, showing reduced magnitude and spatial variability over areas containing cirrus clouds. The cirrus correction algorithm also recovered some areas that were previously screened out by the cloud detection procedure. Comparisons between the cirrus-corrected AOD and AERONET observations revealed that the cirrus correction procedure improved the data quality under thin cirrus and significantly increased the percentage of data within the expected error. In addition, long-term comparisons with CALIOP retrievals over a broad region suggested that the cirrus-corrected AOD provided similar frequency and spatial distributions as the overall data (which included both clear-sky and cirrus-corrected AOD data), whereas the cirrus-contaminated AOD showed significant overestimation. The cirrus correction procedure was also assessed by comparing the MODIS cirrus correction magnitude with the CALIOP COD. The high correlation between the two parameters suggested low random error of the cirrus correction procedure, despite the homogeneity and linearity assumptions in calculating the cirrus reflectance and cirrus-corrected reflectance, respectively.

[38] An advantage of the empirical method used here is that it does not require sophisticated radiative transfer simulations, in this case, incorporating complicated ice crystal properties, which make the simulation less tractable since such quantities are not known a priori on a pixel-by-pixel basis. Consequently, the algorithm was restricted to only optically thin cirrus conditions ($\rho_{1.38} < 0.05$) to which the linear assumption is applicable. Without the linear assumption, the cirrus signal correction in the TOA reflectance requires two-way total transmittance and spherical albedo of the cirrus layer, which should be calculated using a radiative transfer model. A follow-on study is underway to resolve these issues and improve quantification of the AOD uncertainty associated with the cirrus correction process.

[39] In addition, we plan to apply the suggested method to land surfaces using the Deep Blue algorithm [*Hsu et al*., 2004, 2006, 2013]. The method can be applied to bright surfaces as long as sufficient columnar water vapor exists to screen the surface signal. However, scenes with high spatial variability in surface reflectance at visible bands often cause poor correlation between reflectance at 1.38 μm and visible wavelengths, thereby resulting in reduced performance of the algorithm. It is expected that the use of the 0.412 μm band

in calculating cirrus reflectance and extending it to other bands (0.47, 0.65 μm), assuming negligible change in spectral reflectance of thin cirrus across the visible wavelength range, can improve the applicability of the method over land surfaces. To further extend the coverage to low water vapor conditions, additional corrections for surface signals in the 1.38 μm band are required for better accuracy.

[40] Through decreasing the error in retrieved AOD when contaminated by unmasked thin cirrus clouds and expanding spatial coverage by allowing the retrieval of AOD under conditions of thin cirrus which were previously discarded, application of this technique will lead to the improvement of aerosol data sets derived from passive spaceborne imaging radiometers such as MODIS. Given the semipersistent cirrus cloud cover in certain regions (e.g., tropical oceans), this has the potential to significantly increase the utility of these satellite data products. In addition to the more than 10 year time series available from each of the two MODIS sensors, the technique can also be applied to other sensors making measurements at similar wavelengths, such as the Visible and Infrared Imaging Radiometer Suite aboard the Suomi National Polar-orbiting Partnership satellite, launched in late 2011.

[41] **Acknowledgments.** This project was funded by the NASA's EOS program, managed by Hal Maring. The MODIS data were obtained from the Level 1 and Atmosphere Archive and Distribution System (LAADS), and the CALIOP data were obtained from the NASA Langley Research Center Atmospheric Science Data Center. We thank the AERONET staff, PIs, and site managers for their effort in establishing and maintaining Nauru site (B. N. Holben, R. Wagener, L. Jones, and K. Nitschke). The authors are grateful to the anonymous reviewers for their constructive comments and suggestions.

References

Dessler, A. E., and P. Yang (2003), The distribution of tropical thin cirrus clouds inferred from Terra MODIS data, *J. Clim.*, *16*, 1241–1247.

Eck, T. F., et al. (2010), Climatological aspects of the optical properties of fine/coarse mode aerosol mixtures, *J. Geophys. Res.*, *115*, D19205, doi:10.1029/2010JD014002.

Gao, B.-C., Y. J. Kaufman, W. Han, and W. J. Wiscombe (1998), Correction of thin cirrus path radiances in the 0.4–1.0 μm spectral region using the sensitive 1.375 μm cirrus detecting channel, *J. Geophys. Res.*, *103*, 32,169–32,176, doi:10.1029/98JD02006.

Gao, B.-C., Y. J. Kaufman, D. Tanré, and R. R. Li (2002a), Distinguishing tropospheric aerosols from thin cirrus clouds for improved aerosol retrievals using the ratio of 1.38-μm and 1.24-μm channels, *Geophys. Res. Lett.*, *29*(18), 1890, doi:10.1029/2002GL015475.

Gao, B.-C., P. Yang, W. Han, R.-R. Li, and W. J. Wiscombe (2002b), An algorithm using visible and 1.38-μm channels to retrieve cirrus cloud reflectances from aircraft and satellite data, *IEEE Trans. Geosci. Remote Sens.*, *40*(8), 1659–1668.

Holben, B. N., et al. (1998), AERONET—A federated instrument network and data archive for aerosol characterization, *Remote Sens. Environ.*, *66*, 1–16.

Hsu, N. C., J. R. Herman, and S.-C. Tsay (2003), Radiative impacts from biomass burning in the presence of clouds during boreal spring in Southeast Asia, *Geophys. Res. Lett.*, *30*(5), 1224, doi:10.1029/2002GL016485.

Hsu, N. C., S. C. Tsay, M. D. King, and J. R. Herman (2004), Aerosol retrievals over bright-reflecting source regions, *IEEE Trans. Geosci. Remote Sens.*, *42*(3), 557–569.

Hsu, N. C., S. C. Tsay, M. D. King, and J. R. Herman (2006), Deep blue retrievals of Asian aerosol properties during ACE-Asia, *IEEE Trans. Geosci. Remote Sens.*, *44*(11), 3180–3195.

Hsu, N. C., M.-J. Jeong, C. Bettenhausen, A. M. Sayer, R. Hansell, C. S. Seftor, J. Huang, and S.-C. Tsay (2013), Enhanced Deep Blue aerosol retrieval algorithm: The second generation, *J. Geophys. Res. Atmos.*, *118*, 1–20, doi:10.1002/jgrd.50712.

Huang, J., N. C. Hsu, S.-C. Tsay, M.-J. Jeong, B. N. Holben, T. A. Berkoff, and E. J. Welton (2011), Susceptibility of aerosol optical thickness retrievals to thin cirrus contamination during the BASE-ASIA campaign, *J. Geophys. Res.*, *116*, D08214, doi:10.1029/2010JD014910.

Huang, J., et al. (2012), Evaluations of cirrus contamination and screening in ground aerosol observations using collocated lidar systems, *J. Geophys. Res.*, *117*, D15204, doi:10.1029/2012JD017757.

Intergovernmental Panel on Climate Change (2007), Climate Change 2007: The Physical Science Basis, in *Contribution of Working Group I to the Fourth Assessment Report of the Intergovernmental Panel on Climate Change*, edited by S. Solomon et al., Cambridge University Press, Cambridge, United Kingdom and New York, NY, USA.

Jethva, H., O. Torres, L. A. Remer, and P. K. Bhatia (2013), A color ratio method for simultaneous retrieval of aerosol and cloud optical thickness of above-cloud absorbing aerosols from passive sensors: Application to MODIS measurements, *IEEE Trans. Geosci. Remote Sens.*, *51*(7), 3862–3870, doi:10.1109/TGRS.2012.2230008.

Kaufman, Y. J., et al. (2005), A critical examination of the residual cloud contamination and diurnal sampling effects on MODIS estimates of aerosol over ocean, *IEEE Trans. Geosci. Remote Sens.*, *43*(12), 2886–2897.

Kim, S.-W., S. Berthier, J.-C. Raut, P. Chazette, F. Dulac, and S.-C. Yoon (2008), Validation of aerosol and cloud layer structures from the space-borne lidar CALIOP using a ground-based lidar in Seoul, Korea, *Atmos. Chem. Phys.*, *8*, 3705–3720.

Kittaka, C., D. M. Winker, M. A. Vaughan, A. Omar, and L. A. Remer (2011), Intercomparison of column aerosol optical depths from CALIPSO and MODIS-Aqua, *Atmos. Meas. Tech.*, *4*, 131–141, doi:10.5194/amt-4-131-2011.

Kotchenova, S. Y., and E. F. Vermote (2007), Validation of a vector version of the 6S radiative transfer code for atmospheric correction of satellite data. Part II. Homogeneous Lambertian and anisotropic surfaces, *Appl. Opt.*, *46*(20), 4455–4464.

Kotchenova, S. Y., E. F. Vermote, R. Matarrese, and F. J. Klemm (2006), Validation of a vector version of the 6S radiative transfer code for atmospheric correction of satellite data. Part I: Path radiance, *Appl. Opt.*, *45*(26), 6762–6774.

Lee, J., J. Kim, P. Yang, and N. C. Hsu (2012), Improvement of aerosol optical depth retrieval from MODIS spectral reflectance over the global ocean using new aerosol models archived from AERONET inversion data and tri-axial ellipsoidal dust database, *Atmos. Chem. Phys.*, *12*, 7087–7102, doi:10.5194/acp-12-7087-2012.

Levy, R. C., L. A. Remer, S. Mattoo, E. F. Vermote, and Y. J. Kaufman (2007), Second-generation operational algorithm: Retrieval of aerosol properties over land from inversion of Moderate Resolution Imaging Spectroradiometer spectral reflectance, *J. Geophys. Res.*, *112*, D13211, doi:10.1029/2006JD007811.

Mamouri, R. E., V. Amiridis, A. Papayannis, E. Giannakaki, G. Tsaknakis, and D. S. Balis (2009), Validation of CALIPSO space-borne-derived attenuated backscatter coefficient profiles using a ground-based lidar in Athens, Greece, *Atmos. Meas. Tech.*, *2*, 513–522.

Martins, J. V., D. Tanré, L. A. Remer, Y. J. Kaufman, S. Mattoo, and R. Levy (2002), MODIS cloud screening for remote sensing of aerosols over oceans using spatial variability, *Geophys. Res. Lett.*, *29*, 1619, doi:10.1029/2001GL013252.

Mayer, B., and A. Kylling (2005), Technical note: The libRadtran software package for radiative transfer calculations – description and examples of use, *Atmos. Chem. Phys.*, *5*, 1855–1877, doi:10.5194/acp-5-1855-2005.

Meyer, K., and S. Platnick (2010), Utilizing the MODIS 1.38 μm channel for cirrus cloud optical thickness retrievals: Algorithm and retrieval uncertainties, *J. Geophys. Res.*, *115*, D24209, doi:10.1029/2010JD014872.

Meyer, K., P. Yang, and B.-C. Gao (2004), Optical thickness of tropical cirrus clouds derived from the MODIS 0.66- and 1.375-μm channels, *IEEE Trans. Geosci. Remote Sens.*, *42*(4), 833–841.

Meyer, K., P. Yang, and B.-C. Gao (2007), Ice cloud optical depth from MODIS cirrus reflectance, *IEEE Trans. Geosci. Remote Sens.*, *4*(3), 471–474.

Oo, M., and R. Holz (2011), Improving the CALIOP aerosol optical depth using combined MODIS-CALIOP observations and CALIOP integrated attenuated total color ratio, *J. Geophys. Res.*, *116*, D14201, doi:10.1029/2010JD014894.

Pierce, J. R., R. A. Kahn, M. R. Davis, and J. M. Comstock (2010), Detecting thin cirrus in Multiangle Imaging Spectroradiometer aerosol retrievals, *J. Geophys. Res.*, *115*, D08201, doi:10.1029/2009JD013019.

Remer, L. A., et al. (2005), The MODIS aerosol algorithm, products and validation, *J. Atmos. Sci.*, *62*, 947–973.

Remer, L. A., D. Tanré, and Y. J. Kaufman (2006), Algorithm for remote sensing of tropospheric aerosol from MODIS: Collection 5, MODIS Algorithm Theoretical Basis Document, http://modis-atmos.gsfc.nasa.gov/MOD04 L2/atbd.html.

Roskovensky, J. K., and K. N. Liou (2003), Detection of thin cirrus from 1.38 μm/0.65 μm reflectance ratio combined with 8.6–11 μm brightness temperature difference, *Geophys. Res. Lett.*, *30*(19), 1985, doi:10.1029/2003GL018135.

Roskovensky, J. K., and K. N. Liou (2005), Differentiating airborne dust from cirrus clouds using MODIS data, *Geophys. Res. Lett.*, *32*, L12809, doi:10.1029/2005GL022798.

Roskovensky, J. K., and K. N. Liou (2006), Simultaneous determination of aerosol and thin cirrus optical depths over oceans from MODIS data: Some case studies, *J. Atmos. Sci.*, *63*, 2307–2323.

Roskovensky, J. K., K. N. Liou, T. J. Garrett, and D. Baumgardner (2004), Simultaneous retrieval of aerosol and thin cirrus optical depths using MODIS airborne simulator data during CRYSTAL-FACE and CLAMS, *Geophys. Res. Lett.*, *31*, L18110, doi:10.1029/2004GL020457.

Sassen, K., Z. Wang, and D. Liu (2008), Global distribution of cirrus clouds from CloudSat/Cloud-Aerosol Lidar and Infrared Pathfinder Satellite Observations (CALIPSO) measurements, *J. Geophys. Res.*, *113*, D00A12, doi:10.1029/2008JD009972.

Sayer, A. M., A. Smirnov, N. C. Hsu, and B. N. Holben (2012), A pure marine aerosol model, for use in remote sensing applications, *J. Geophys. Res.*, *117*, D05213, doi:10.1029/2011JD016689.

Schuster, G. L., M. Vaughan, D. MacDonnell, W. Su, D. Winker, O. Dubovik, T. Lapyonok, and C. Trepte (2012), Comparison of CALIPSO aerosol optical depth retrievals to AERONET measurements, and a climatology for the lidar ratio of dust, *Atmos. Chem. Phys.*, *12*, 7431–7452, doi:10.5194/acp-12-7431-2012.

Smirnov, A., B. N. Holben, T. F. Eck, O. Dubovik, and I. Slutsker (2000), Cloud-screening and quality control algorithms for the AERONET database, *Remote Sens. Environ.*, *73*, 337–349, doi:10.1016/S0034-4257(00)00109-7.

Stamnes, K., S. Tsay, W. Wiscombe, and K. Jayaweera (1988), Numerically stable algorithm for discrete-ordinate-method radiative transfer in multiple scattering and emitting layered media, *Appl. Opt.*, *27*, 2502–2509.

Torres, O., H. Jethva, and P. K. Bhartia (2012), Retrieval of aerosol optical depth above clouds from OMI observations: Sensitivity analysis and case studies, *J. Atmos. Sci.*, *69*, 1037–1053.

Winker, D. M., M. A. Vaughan, A. Omar, Y. Hu, K. A. Powell, Z. Liu, W. H. Hunt, and S. A. Young (2009), Overview of the CALIPSO mission and CALIOP data processing algorithms, *J. Atmos. Oceanic Technol.*, *26*, 2310–2323, doi:10.1175/2009JTECHA1281.1.

Wu, D. L., J. H. Chae, A. Lambert, and F. F. Zhang (2011), Characteristics of CALIOP attenuated backscatter noise: Implication for cloud/aerosol detection, *Atmos. Chem. Phys.*, *11*, 2641–2654, doi:10.5194/acp-11-2641-2011.